

To: *Rita Ballard / Joe Youngblood*
MS 62355

SURFACE REFLECTANCE CORRECTION AND STEREO ENHANCEMENT
OF LANDSAT THEMATIC MAPPER IMAGERY FOR STRUCTURAL GEOLOGIC EXPLORATION*

Richard L. Thiessen and Lisa K. Johnson
Geology Department, Washington State University, Pullman, Washington, USA
and
Harlan P. Foote and Jay R. Eliason
Pacific Northwest Laboratory, Richland, Washington, USA

ABSTRACT

Structural remote sensing analysis techniques for exploration have focussed on mapping of crustal fracture zones which can provide pathways for mineralization as well as permeability for movement and/or accumulation of oil, gas, and geothermal fluids. These analyses have relied heavily on manual lineament analysis of enhanced imagery. These image products contain shadow effects that preferentially enhance or suppress lineaments. This study was conducted to evaluate a digital technique for surface reflectance correction for shadows and subsequent stereo enhancement to provide shadow corrected stereo models for structural geologic exploration.

The appearance of lineaments on imagery is controlled by many factors. These include surface spectral reflectance, as determined by lithologies, soil types, and vegetation; shadowing effects caused by illumination of the irregular surface from a point source; and topographic relief patterns (for stereopairs). In order to examine the relative importance of each of these factors, image products were developed that isolate each effect. These products were produced from digital Landsat Thematic Mapper (TM) data and a digital elevation model (DEM). The Paiute Ridge quadrangle, Nevada, was selected as a test area for the analysis.

Landsat TM data were registered to the DEM and processed to reduce topographic shadowing effects. A Minnaert reflectance model was used to approximate the topographic lighting effects. This reflectance model provided quantitative evaluation of each pixel in the image and was directly used to create a shadow image. These reflectance values were utilized to remove shadow effects from the TM data to produce the corrected surface reflectance. The DEM was used to stereo enhance the shadow corrected TM image.

Lineament analysis of the original and enhanced image products was conducted by multiple interpreters and compared with geologic maps, field measurements of fractures, and reported data available for the test area. Digitally computed crustal fracture planes from DEM analysis of the test area were also used for comparison with the lineaments. Fracture orientations determined from the original TM and shadow images show similar bias resulting from solar illumination. This bias was not present in the results from the shadow corrected and the corrected stereopair images, with the best correlation to the trends observed in the field data given by the latter. These results also matched the crustal fracture plane orientations computed directly from the DEM. In addition, the lineaments were directly correlated to faults by location as well as orientation. Analysis of the original image yielded the poorest percentages of faults correctly picked and the poorest percentages of lineaments that matched the faults. Conversely, the corrected stereopair gave the best results, indicating that it is a superior product for lineament analysis.

* Presented at the Fifth Thematic Conference: "Remote Sensing for Exploration Geology," Reno, Nevada, September 29-October 1, 1986.

8712030272 871109
PDR WASTE
WM-10 PDR

1. INTRODUCTION

Analysis of lineaments utilizing air photos and space images has become a common exploration practice. Numerous workers have shown that a low angle of solar illumination will accentuate subtle topographic features and so aid in the detection of lineaments. Hackman (1967), Wise (1968, 1969), Slemmons (1969), Walker and Trexler (1977), Dean (1982), Larson (1982), and Moore and Weitz (1983) have all discussed the advantages of oblique illumination. However, low-angle illumination appears to produce a strong bias on the trends of the observed structures (Wise, 1969, 1983; Sawatzky and Lee, 1974; Siegal, 1977; Eliason, 1984). Features that are parallel to the angle of illumination are not as easily detected as those at 30° and 90° angles. The shadowing effect also detracts from automated lineament enhancement procedures, such as Moore and Waltz's (1983) digital convolution technique. A technique is therefore required which will correct for and remove this undesirable shadowing effect.

Minnaert (1961), Horn (1981), Justice et al. (1981), Hugli and Frei (1983), and Foote et al. (in review) have devised techniques based on digital elevation models (DEMs) which determine the shading for each pixel in each spectral band. Reflectance models are created that simulate a uniform grey surface of variable orientation that interacts with the solar illumination direction. These reflectance models are used to create images of shadows that are based solely on the topographic effect. These images are then ratioed with a Landsat Thematic Mapper (TM) image to create a shadow corrected image. Lineaments observed on this new image should not have any of the shadowing biases that have existed in previous lineament studies. However, this correction process also sacrifices the positive aspects of the shadowing. Lineaments that are expressed as topographic features would have been preferentially enhanced by the shadows. In order to regain the topographic effect, the corrected image can be combined with the DEM data set in order to produce a stereopair of the corrected image. The topography will then appear as three dimensional relief.

This paper contains a discussion of the applicability of shadow corrected images for structural geologic exploration studies. Lineament analysis of four different images: an original TM image, the shadow corrected image, the shadowing effect by itself, and the corrected stereopair will be used to demonstrate the advantages of the shadow correction technique.

2. STUDY SITE

The Paiute Ridge quadrangle in southwestern Nevada was chosen as a study site because of the minimal amount of vegetation in the region and because of the existence of a U.S. Geological Survey 1:24,000 scale geologic map for the quadrangle (Byers and Barnes, 1967). The Paiute Ridge is directly to the east of Yucca Flat and is within the Nevada Test Site. The study area is underlain by Paleozoic sedimentary rocks and late Tertiary volcanic tuffs, clastics, and basalts. Faults are quite common and appear to be oriented in two directions. The late Tertiary lithologies show a very strong north-northwest (NNW) orientation (Fig. 1a) which is typical of Basin and Range extensional structures in this region. Faults in the Paleozoic rocks show this trend as well as a subparallel north-northeast trend (NNE). There is also an additional east-west (EW) concentration (Fig. 1b). Ekren et al. (1968), working elsewhere in the Nevada Test Site, observed similar relations but observed the older sets involving rocks as young as 17 million years old.

Barosh (1968) mapped fractures that were created during weapons tests on Yucca Flat. These tests produced well developed fracture sets that show the NNW trend (Fig. 1c). However, a much stronger northeast (NE) orientation is observed. First motion studies of natural and induced earthquakes at the Nevada Test Site (Hamilton and Healey, 1969), as well as in southern Nevada and

adjacent California (Rogers and Lee, 1976; Smith and Lindh, 1978) show two characteristic patterns. The first pattern is compatible with extensional faulting along the NE fracture trend. The second pattern substantiates right lateral strike slip faulting parallel to the NNW orientation. This faulting would indicate reactivation or earlier Basin and Range extensional structures. Both of these solutions are possible in the current stress field which is characterized by a northwesterly extensional direction (Zoback and Zoback, 1980). The progressive rotation of the stress field, as indicated by the three fracture sets, has been observed elsewhere in southern Nevada by Ander (1984) and Angelier et al. (1985).

3. PRODUCTION OF IMAGES

Four different images were utilized in this study. These images included the original TM, a corrected version in which the shadows were removed, an image composed of just the shadows superimposed on a uniform grey surface, and a stereopair of the corrected TM image. All image products were prepared by the Pacific Northwest Laboratory in Richland, Washington, USA. Scales of the images varied from 1:54,700 to 1:58,400. The original TM image for the Paiute Ridge quadrangle was collected on March 23, 1984, and had a moderately oblique solar illumination angle of 42° from the southeast. The image was registered to a topographic map, nearest neighbor resampled into a north-south east-west grid, enhanced with linear contrast stretches and clipped to the size of the quadrangle. TM bands 1, 4 and 7 were utilized.

No detailed DEM existed for the quadrangle; consequently the U.S. Geological Survey's 1:24,000 scale topographic map (6.1 m or 20' contour interval) was manually digitized and elevations were interpolated to match the TM image's grid spacing. Non-Lambertian reflectance models, as discussed by Minnaert (1961) and Horn (1981), were applied to each individual spectral band. The exponent constant, K , ranged from 0.85 to 0.92 for the various bands, indicating reflectance models that were close to the Lambertian model ($K = 1.0$). See Foote et al. (in review) for a more detailed discussion of the process. These reflectance models were then ratioed into the original TM bands in order to produce a shadow corrected image. The colors of the various lithologies were not changed from the original image, however, the shadows were effectively removed from it. This alleviated considerable confusion between various darker lithologies, such as basalts, and the shadows.

The third image was produced by simply applying the reflectance model to a uniform grey background to create an image showing just the shadows. To create the fourth image, the DEM data set was used to shift the pixels of the corrected image relative to their elevation. This resulted in a stereopair of the corrected image.

Each of the above images has a different combination of three effects controlling the appearance of the lineaments. These effects include the shadowing effect, the spectral changes caused by geologic and other surface effects, and topographic relief effects. The original image demonstrates the combined effects of the spectral and shadow controls. The corrected image only displays the influence of the spectral signatures. Similarly, the shadow image is controlled exclusively by the shadow effect. The corrected stereopair shows the spectral control combined with the topography. The three-dimensionality of the stereo model enabled the interpreters to have the benefit of the topographic effect without having the adverse shadowing effect. We attempted to make a fifth image which was a stereopair of random dots, with the DEM controlling the stereo effect. This image should have shown purely the topographic effect. Unfortunately, the random dots proved difficult to focus on, and so this method was abandoned.

4. DEM FRACTURES

Eliason (1984), Eliason and Eliason (1985), and Eliason and Thiessen (1986) have developed an independent fracture analysis technique that is based solely on the topographic data set. The fundamental concept of this process is that major fractures and faults will control the alignment of stream drainages. Computer programs have been written to search for these lows in the topography of a DEM and produce vectors along the stream valley bottoms. Another program tests for sets of vectors that are coplanar and, therefore, are possibly controlled by the same fracture plane. The three-dimensional orientation and location of this plane is calculated by the program. These programs are still in the developmental stage, but preliminary runs on the Paiute Ridge DEM data set produced the same three fracture orientations (Fig. 1d) that the mapped faults (Fig. 1a and 1b) and explosion induced fractures show (Fig. 1c). This technique has the advantage of determining fracture orientations independent of any solar illumination problems, as well as variations between individual analyst's interpretations. However, the results are still preliminary and improved software routines are being developed.

5. LINEAMENT ANALYSIS OF IMAGES

Five interpreters analyzed each of the four images. Their maps were then combined into a single compilation map (designated 3/5) for each image on which are shown only those lineaments or segments that were identified by at least three out of the five interpreters. These are felt to be the structures of higher confidence because of their repeatability. The orientations observed on these compilations are shown in the bottom row of Figure 1. Lineaments observed on the original image (Fig. 1e) show a strong north-south orientation with two separate spikes, one that matches the NNW orientation of the mapped faults and one that is oriented just east of north (NNE). The NE and EW sets show up but are rather subdued. The shadow image (Fig. 1f) shows the NNW, EW and NE sets all quite well. A strong peak due north-south also exists, which is mostly a result of the shadow biasing effect. A gap is observed in the lineaments oriented west-northwest and is centered on the illumination direction. This gap is partially real (as can be seen by all the other rose diagrams), but on the shadow image it is particularly well developed. This graphically depicts the inability to see lineaments subparallel to the illumination direction when they are defined solely by shadows. Most of the maxima observed in the shadow image are partially controlled by the solar illumination effect. The NNW and EW sets are at a 30° angle to the sun and are quite well developed. The NE set is perpendicular to it. The north-south spike is a bit of an enigma because it is approximately at a 60° angle to the illumination. This orientation also occurs in the original image, although it is slightly east of due north (the NNE trend). Several of the other rose diagrams in this report (Figs. 1b, 1d, and 1e) also show this trend, but it is more subdued. Apparently, this is a secondary structural trend that is amplified on the original and shadow images because of their shadow bias effect.

The rose diagram for the shadow corrected image (Fig. 1g) is dominated by the NNW trend with well developed NE and EW trends. This diagram also shows the NNE trend, indicating that this orientation is partially real on the original and shadow image. The corrected stereopair (Fig. 1h) shows essentially the same pattern, with the NNW trend dominant, the NE and EW trends strong, and the NNE trend subdued. Both of these rose diagrams can be produced by combining the NNW, EW and NNE orientations of the faults observed in the Tertiary and Paleozoic rocks (Figs. 1a and 1b) and the present day NE fractures shown by the weapons tests (Fig. 1c). The rose diagrams also match the orientations observed in the DEM fractures (Fig. 1d). The latter have been determined independently of any shadow effect. Inspection of the rose diagrams for the original and shadow images shows that they do not match this

combination as well, but instead resemble each other and display the adverse effects of using images that have shadows in them.

6. CORRELATION OF FAULTS TO LINEAMENTS

The lineament traces of each interpreter, as well as the 3/5 compilation lineaments, were compared directly to the mapped faults. Those lineaments or portions thereof which matched a fault's location and orientation were flagged as being correlated. Tables 1 and 2 give the statistics of correlations where Table 1 lists cumulative lengths in kilometers and Table 2 gives numbers of lineaments. For each of the four images, the amount of lineaments that matched the faults is given in the first row. The second row gives the original total amount of lineaments (correlated and uncorrelated) on that particular map. The third row gives the percentage of faults correctly picked by the lineament map. This is equal to the amount of correlated lineaments (which equals the amount of correlated faults) divided by the total amount of mapped faults. The published map of the quadrangle had 685 faults on it with a cumulative length of 291.20 km. The fourth row shows the percentage of the lineaments that were correct, which is equal to the amount of correlated lineaments divided by the total amount of lineaments for that map. Data are given for each of the five individual interpreters. The most significant values are for the 3/5 compilations; hence these will be discussed in more detail. For all of the images, the 3/5 compilation for the original image had the lowest percentage of faults and lineaments correct [for both length (Table 1) and numbers (Table 2)]. In all cases, the corrected stereopair had the highest percentages. The percentages for the shadow image and corrected image were between the corrected stereopair maximum and the 3/5 compilation minimum.

The average length of the mapped faults in the Paiute Ridge quadrangle is 0.425 km (0.264 mi). Interpreter number one's picks were correlated to faults of successively longer lengths in order to test if all of the longer faults were being picked. When number of faults are considered, there is a significant increase in the percentage of faults correctly picked from 27.7% for faults of all lengths to 64.7% for faults at least 1.61 km (1.00 mi) long. This indicates that the major structures are detected by lineament analysis.

The repeatability of this lineament analysis is indicated by Tables 1 and 2. For the individual interpreters, the average of the cumulative lengths of the structures observed ranged from 220 km to 336 km. This average can be compared to the 3/5 compilation, where the cumulative lengths for the various images ran from 129 km to 151 km. If number of structures is considered, the averages of the individuals were from 272 to 346 lineaments, versus 204 to 220 for the 3/5 compilation. Therefore, there is a considerable amount of matching between the individual interpreters causing the amounts on the compilations to be on the order of half of the individual interpretations.

Figure 2a shows the faults found on the published map of the quadrangle. All of the correlated lineaments for the individual interpreters are displayed in Figure 2b. Most of the faults that were detected were not observed just once or twice but numerous times; this again indicates that the interpretations are highly repeatable in many cases.

7. FIELD VERIFICATION

With five interpreters working on four images, each structure could be observed up to 20 times. During a visit to the northwest portion of the Paiute Ridge quadrangle we checked on several features that were detected a large number of times. One feature, observed 14 times, proved to be a basalt dike. A clastic streamer in stream sediments was flagged 13 times, a darker layer in the carbonate unit was seen 16 times, and a carbonate/tuff contact was identified 15 times. Several parallel faults were found in an excavation pit

in a northeast-oriented stream valley. This valley was flagged as a lineament 15 times and did not align with a previously mapped fault.

During the field visit, the orientations of numerous joints, filled joints, open joints, and faults were measured. Figure 3 is a uniform distribution contoured stereonet of the poles to the observed structures. This figure shows that most of the features are nearly vertical, and define three orientations. The EW trend is dominant, with NE and NNE trends as subsidiary orientations. These trends align with those observed in the previously mapped faults (Figs. 1a and 1b), weapons test fractures (Fig. 1c), DEM fractures (Fig. 1d), and lineament analyses of the corrected and corrected stereopair images (Figs. 1g and 1h). Open and filled joints occur in all three directions, whereas faults best defined the NNW orientation.

8. CONCLUSIONS

Four images were used to test the applicability of removing shadows from images before lineament analysis. These images were an original Thematic Mapper (TM) image, a shadow corrected TM image, an image of just the shadows, and a stereopair of the shadow corrected TM image. Orientations were compared to those of previously mapped faults as well as fractures induced by adjacent weapons tests. The best correlations of analyses with field data were obtained with the shadow corrected stereopair and the shadow corrected image. The shadow image and the original image with their biases due to sun angle effects correlated poorly with known trends. Lineaments were also directly correlated to mapped faults by position in addition to orientation. Statistics were compiled on the length and number of faults that were correctly identified and on the length and number of lineaments that matched the faults. The corrected stereopair consistently gave the best results and the original image gave the worst. The shadow and corrected images were moderately successful. These analyses show that the corrected stereopair is by far the superior product for lineament analysis and the original image is consistently the worst. The original image has two effects defining lineaments, the shadow effect caused by topographic relief combined with the sun angle, and the spectral response of the surface, which is controlled by the geology and additional factors. The corrected stereopair shows the surface spectral response and topographic relief; however, the latter is expressed as pure three-dimensionality, not as shadows with their adverse effects on observed orientations. This three dimensionality is vital to see structures that are predominantly topographic in nature.

We are currently in the process of testing these shadow corrected TM bands for lithologic identification. Classifications by analysts, as well as machine classifications, are being done. The spectral signatures of representative hand samples collected in the field are also being incorporated in the analyses.

9. ACKNOWLEDGMENTS

We gratefully acknowledge the assistance of the interpreters of the images: John Reed, J.B. Lim, Charles Pitz, and Erik Weberg. We also thank Greg Mohl, Eric Rieken, and Craig Brouger for assistance with the graphics, and Eric Rieken and Dennis Beaver for a critical review of the manuscript. The work was partially supported by the U.S. Department of Energy under contract DE-AC06-76RLO 1830.

10. REFERENCES

Ander, H.D., 1984, Rotation of Late Cenozoic extensional stresses, Yucca Flat region, Nevada Test Site, Nevada: Ph.D. Thesis, Rice Univ., Houston, TX.

- Angelier, J., B. Colletta, and R.E. Anderson, 1985, Neogene paleostress changes in the Basin and Range: A case study at Hoover Dam, Nevada-Arizona: Geological Society of America Bulletin, v. 96, p. 347-361.
- Barosh, P.J., 1968, Relationships of explosion-produced fracture patterns to geologic structure in Yucca Flat, Nevada Test Site: Geological Society of America Memoir, no. 110, p. 199-218.
- Byers, F.M., and H. Barnes, 1967, Geologic map of the Paiute Ridge quadrangle, Nye and Lincoln Counties, Nevada: U.S. Geological Survey Geologic Quadrangle Map GQ-577, 1:24,000 scale.
- Dean, K., 1982, Enhancement of satellite imagery for interpretation of linear features: Second Thematic Conference on Remote Sensing for Exploration Geology, p. 303-304.
- Ekren, E.B., C.L. Rogers, R.E. Anderson, and P.P. Orkild, 1968, Age of basin and range normal faults in the Nevada Site and Nellis Air Force Range, Nevada: Geological Society of America Memoir, no. 110, p. 247-250.
- Eliason, J.R., 1984, A technique for structural geologic analysis of topography: Ph.D. Thesis, Washington State Univ., Pullman, WA.
- Eliason, J.R., and V.E. Eliason, 1985, A comparative study of fracture planes computed from topography and lineaments from imagery with structures and mineralization in the Magnesite Belt of Washington State: Fourth Thematic Conference on Remote Sensing for Exploration Geology, p. 655-664.
- Eliason, J.R., and R.L. Thiessen, 1986, Geologic spatial analysis - a new multiple data source exploration tool: Fifth Thematic Conference on Remote Sensing for Exploration Geology (this volume).
- Foote, H.P., R.L. Thiessen, J.R. Eliason, and G.E. Wukelic, in review, Advanced techniques for lithologic and fracture analysis utilizing Thematic Mapper and topographic data: Photogrammetric Engineering and Remote Sensing.
- Hackman, R.J., 1967, Time, shadows, terrain and photointerpretation: Geological Survey Research 1967: U.S. Geological Survey Professional Paper 575-B, p. B155-B160.
- Hamilton, R.M., and J.H. Healy, 1969, Aftershocks of the Benham nuclear explosion: Seismological Society of America Bulletin, v. 59, p. 2271-2281.
- Horn, B.K.P., 1981, Hill shading and reflectance map: Proceedings of the IFEE, v. 69, no. 1.
- Hugli, H., and W. Frei, 1983, Understanding anisotropic reflectance in mountainous terrain: Photogrammetric Engineering and Remote Sensing, v. 49, p. 671-683.
- Justice, C.O., S.W. Wharton, and B.N. Holben, 1981, Application of digital terrain data to quantify and reduce the topographic effect on Landsat data: International Journal of Remote Sensing, v. 2, p. 213-230.
- Larson, B.S., 1982, Examination of some factors used in selecting Landsat imagery for lineament interpretation: Second Thematic Conference on Remote Sensing for Exploration Geology, p. 293-302.
- Minnaert, M., 1961, The Solar System, v. 3, p. 213-249, G.P. Kulper, ed., Univ. of Chicago Press.

- Moore, G.K., and F.A. Waltz, 1983, Objective procedures for lineament enhancement and extraction: *Photogrammetric Engineering and Remote Sensing*, v. 49, p. 641-647.
- Rogers, A.M., and H.K. Lee, 1976, Seismic study of earthquakes in the Lake Mead, Nevada-Arizona region: *Seismological Society of America Bulletin*, v. 66, p. 1657-1681.
- Sawatzky, D.L., and K. Lee, 1974, New uses of shadow enhancement: *Remote Sensing of Earth Resources*, v. 3, p. 1-18.
- Siegal, B.S., 1977, Significance of operator variation and the angle of illumination in lineament analysis on synoptic images: *Modern Geology*, v. 6, p. 75-85.
- Slemmons, D.B., 1969, New methods of studying seismicity and surface faulting: *EOS*, v. 50, p. 397-398.
- Smith, R.B., and A.G. Lindh, 1978, Fault-plane solutions of the western United States: A compilation: *Geological Society of America Memoir*, no. 152, p. 107-109.
- Walker, P.M., and D.T. Trexler, 1977, Low sun-angle photography: *Photogrammetric Engineering and Remote Sensing*, v. 43, p. 493-505.
- Wise, D.U., 1968, Regional and sub-continental sized fracture systems detectable by topographic shadow techniques: *Conference on Research in Tectonics*, *Geologic Survey of Canada*, GSC Paper 68-52, p. 175-198.
- Wise, D.U., 1969, Pseudo-radar topographic shadowing for detection of subcontinental sized fracture systems: *Sixth International Symposium on Remote Sensing of the Environment*, Univ. Michigan, p. 603-615.
- Wise, D.U., 1983, Topographic lineaments, shadows, radar, and sandpaper: Attempts to quantify some illusions: *Geological Survey of America Abstracts with Programs*, v. 15, p. 721.
- Zoback, M.L., and M. Zoback, 1980, State of stress in the conterminous United States: *Journal of Geophysical Research*, v. 85, p. 6113-6156.

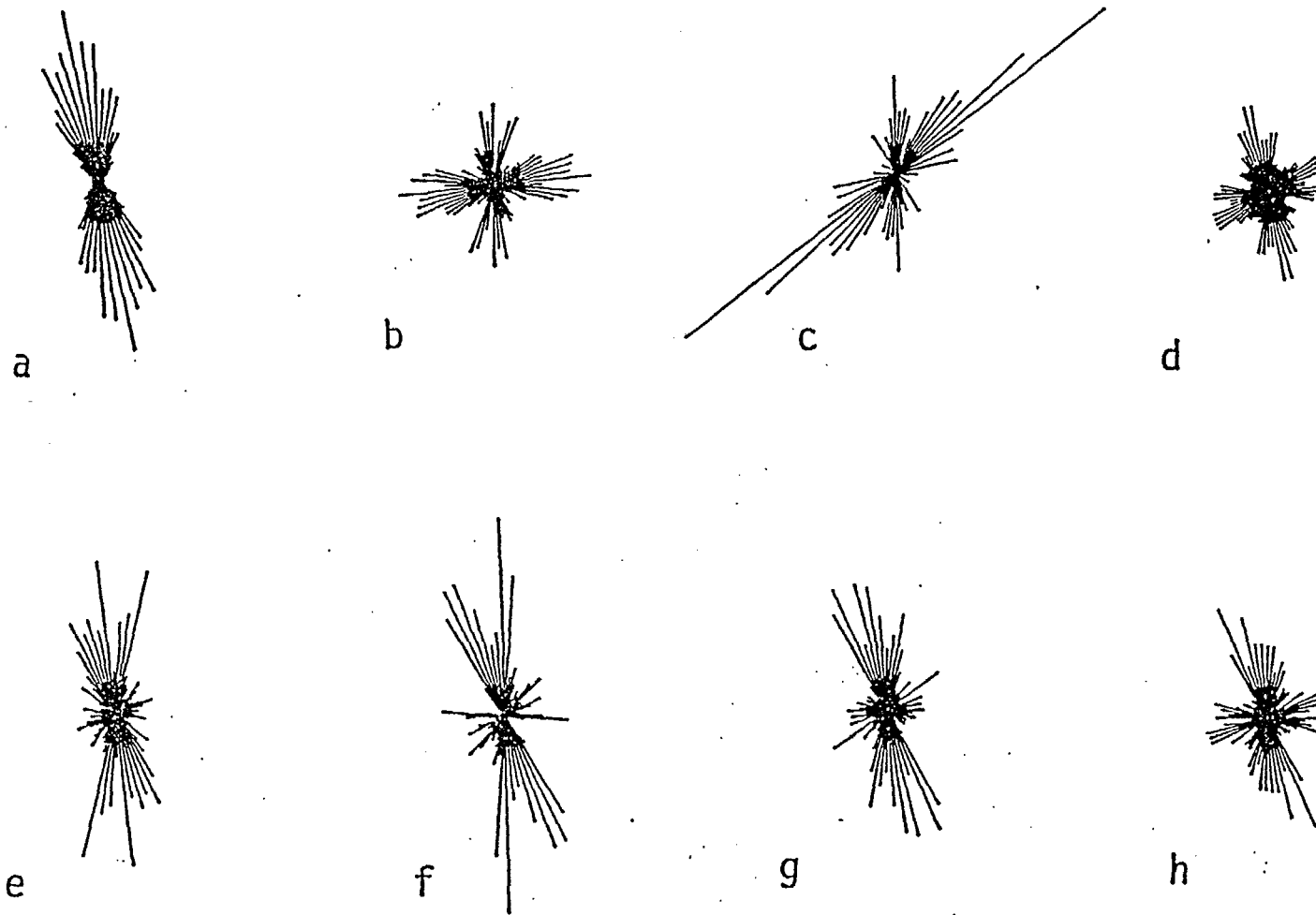


Figure 1. Rose diagrams of: a) Mapped faults in Tertiary lithologies, b) faults in Paleozoic lithologies, c) explosion induced fractures, d) DEM fractures, e) 3/5 compilation lineaments from original image, f) 3/5 for shadow image, g) 3/5 for corrected image, h) 3/5 for corrected stereopair.

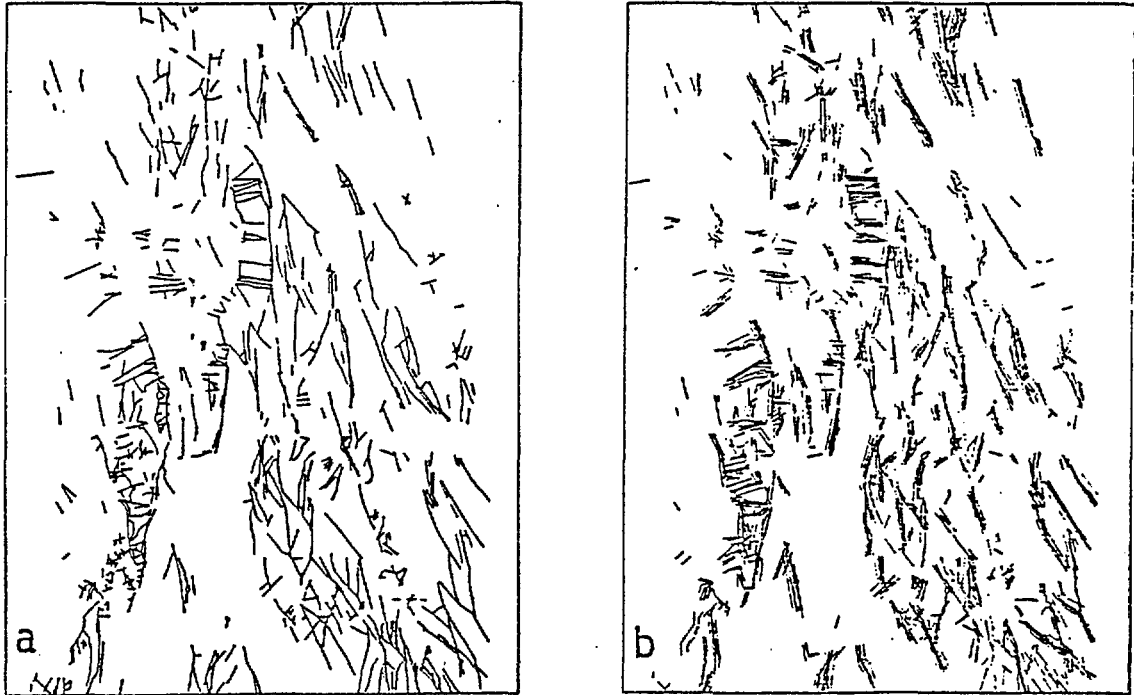


Figure 2. a) Mapped faults in the Paiute Ridge quadrangle.
 b) All correlations to mapped faults for the individual interpreters.

CONTOURS AT 1, 5, AND 10%
 OF POLES TO THE STRUCTURES

PAIUTE RIDGE
 FIELD MAPPED
 JOINTS AND
 FAULTS

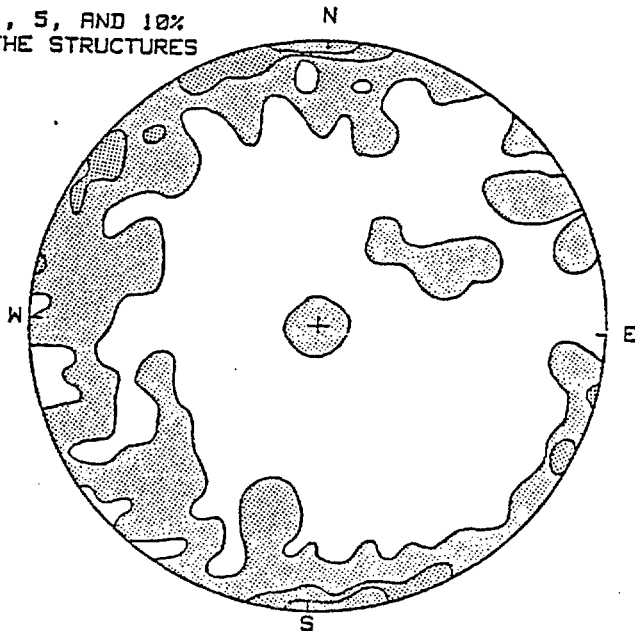


Figure 3.

Contoured stereonet of
 poles to joints, filled
 joints, open joints, and
 faults measured in the
 field.

IMAGE		#1	#2	#3	#4	#5	3/5	AVERAGE	
TABLE 1 -	ORIGINAL	CORRELATED LINS	40.19	32.07	54.30	41.99	52.39	29.64	44.19
Lineament statistics	>	ORIGINAL LINS	220.21	131.26	290.97	243.44	220.16	151.13	221.21
by cumulative lengths.	>	% FAULTS correct	13.81	11.02	18.66	14.43	18.00	10.18	15.18
	>	% LINS correct	18.25	24.43	18.66	17.25	23.80	19.61	20.48
	CORRECTED	CORRELATED LINS	55.30	15.70	47.39	51.62	49.53	33.08	43.91
	>	ORIGINAL LINS	322.80	76.80	338.28	297.49	228.00	150.59	252.67
	>	% FAULTS correct	19.00	5.40	16.28	17.74	17.02	11.37	15.09
	>	% LINS correct	17.13	20.45	14.01	17.35	21.72	21.97	18.13
	SHADOW	CORRELATED LINS	40.71	35.57	70.49	42.03	55.19	30.01	48.80
	>	ORIGINAL LINS	268.83	157.33	306.19	160.63	207.37	129.28	220.07
	>	% FAULTS correct	13.99	12.22	24.22	14.44	18.96	10.31	16.77
	>	% LINS correct	15.14	22.61	23.02	26.16	26.61	23.21	22.71
	CORRECTED	CORRELATED LINS	77.10	31.01	39.57	47.48	58.29	35.20	50.69
STEREOPAIR	>	ORIGINAL LINS	509.30	216.64	321.85	371.12	261.72	150.43	336.12
	>	% FAULTS correct	26.49	10.65	13.60	16.32	20.03	12.10	17.42
	>	% LINS correct	15.14	14.31	12.29	12.79	22.27	23.40	15.36

IMAGE		#1	#2	#3	#4	#5	3/5	AVERAGE	
TABLE 2 -	ORIGINAL	CORRELATED LINS	90.00	96.00	125.00	134.00	130.00	82.00	115.00
Lineament statistics	>	ORIGINAL LINS	224.00	159.00	354.00	415.00	209.00	207.00	272.20
by number of	>	% FAULTS correct	13.14	14.01	18.25	19.56	18.98	11.97	16.79
structures.	>	% LINS correct	40.18	60.38	35.31	32.29	62.20	39.61	46.07
	CORRECTED	CORRELATED LINS	142.00	51.00	108.00	138.00	121.00	90.00	112.00
	>	ORIGINAL LINS	392.00	80.00	449.00	333.00	165.00	204.00	283.80
	>	% FAULTS correct	20.73	7.45	15.77	20.15	17.66	13.14	16.35
	>	% LINS correct	36.22	63.75	24.05	41.44	73.33	44.12	47.76
	SHADOW	CORRELATED LINS	105.00	132.00	153.00	124.00	137.00	96.00	130.20
	>	ORIGINAL LINS	379.00	296.00	379.00	284.00	220.00	220.00	311.60
	>	% FAULTS correct	15.33	19.27	22.34	18.10	20.00	14.01	19.01
	>	% LINS correct	27.70	44.59	40.37	43.66	62.27	43.64	43.72
	CORRECTED	CORRELATED LINS	190.00	67.00	86.00	123.00	137.00	101.00	120.60
STEREOPAIR	>	ORIGINAL LINS	455.00	297.00	381.00	389.00	211.00	204.00	346.60
	>	% FAULTS correct	27.74	9.78	12.55	17.96	20.00	14.74	17.61
	>	% LINS correct	41.76	22.56	22.57	31.62	64.93	49.51	36.69

WM DOCKET CONTROL
CENTER

'87 NOV -9 A9:45

WM Record File

101

WM Project

10

Docket No.

PDR

X LPDR

(B)

Distribution:

R Ballard Youngblood

(Return to WM, 823-SS)

From: Cook, nkc

2740